1988

Steady state dendritic growth of NH4Br from solution

A. Dougherty

Jerry P. Gollub
Haverford College

Steady-state dendritic growth of NH_4Br from solution

A. Dougherty and J. P. Gollub
Department of Physics, Haverford College, Haverford, Pennsylvania 19041-1392
and Department of Physics, University of Pennsylvania, Philadelphia, Pennsylvania 19104-6396
(Received 4 January 1988; revised manuscript received 10 May 1988)

The growth of NH_4Br dendrites from supersaturated aqueous solution is investigated to test recent theories of dendritic growth. A key prediction of these theories is that the tip radius ρ and steady-state growth speed v depend strongly on the surface tension anisotropy ε. We measure the capillary length $\bar{d}_0$ and the crystalline anisotropy of NH_4Br, along with the radius and speed of steady-state dendritic tips, in order to make a quantitative test of the theory. The stability constant σ^* (defined to be $2\bar{d}_0 D/v\rho^2$, where D is the diffusion constant) is found to be 0.081 ± 0.02 for this material, in approximate agreement with the theoretical prediction of 0.065 ± 0.02. The initial side-branch wavelength is found to be slightly larger than predicted. These measurements are consistent with the hypothesis that "microscopic solvability" determines the steady state of a dendrite.

I. INTRODUCTION

Dendritic crystal growth has been the subject of intensive study in recent years as an example of pattern formation in a nonequilibrium system.[1,2] Experiments[3–7] have shown that, for a given material, the steady-state dendrite tip speed v and radius ρ are given uniquely by the driving supersaturation Δ. Furthermore, it is found that the combination $v\rho^2$ is approximately constant, and that the mean side-branch spacing near the tip λ is approximately proportional to ρ. A complete theoretical explanation of these steady-state properties, however, has only recently been proposed.[8–16]

Recent theoretical work, first on two-dimensional local models, and subsequently on three-dimensional nonlocal models of crystal growth, has focused on the proposed mechanism of "microscopic solvability," by which the microscopic length scale set by the surface tension determines the macroscopic scale of the pattern. One of the main predictions of this work is that v and ρ are strong functions of the anisotropy ε in the surface tension.[8–10]

The complex time-dependent behavior of the side branches is less well understood. Numerical[11–13] and analytical[14–16] treatments suggest that side branches could result from the amplification of microscopic fluctuations near the tip. This hypothesis is consistent with the results of a previous experiment,[17] where it was found that side branching is characterized by a broad range of wavelengths, and that side branches on opposite sides of a dendrite are imperfectly correlated. The mean initial side-branch wavelength is predicted to be proportional to ρ, with the ratio λ/ρ a function of the crystalline anisotropy.

However, these predictions have not been adequately tested experimentally. To date, the most completely characterized experiments on free dendritic growth are those of Glicksman and co-workers on succinonitrile.[3–6] To fully test the theory, it is necessary to measure dendritic growth in a material with a different anisotropy, and to use particular care in measuring ε.

In this paper we report experiments on the steady-state dendritic growth of ammonium bromide from supersaturated aqueous solution. We have measured ρ, v, λ, and the materials parameters necessary to make a quantitative test of the theory. We find that, to within the experimental precision, the predictions for the steady-state tip radius and speed are consistent with the experiment, but the prediction for the initial side-branch spacing is slightly smaller than the experimental value.

The organization of this paper is as follows. In Sec. II we summarize the theory of dendritic growth and the method used to measure the capillary length and anisotropy. In Sec. III we describe the experimental apparatus and techniques. The results are presented in Sec. IV and discussed in Sec. V.

II. BACKGROUND

A. Continuum model

For many materials growing from supersaturated solution or from a supercooled melt, a crystal with a smooth, nearly parabolic dendritic tip propagates at constant velocity.[1,2] An example is shown in Fig. 1, where the contours of a dendrite with $\rho=2.3\ \mu$m growing at $v=2.9\ \mu$m/s are shown at 10-s intervals. Behind the tip, a train of time-dependent side branches develops. For cubic materials such as ammonium bromide, four sets of side branches typically grow in the $\langle 100 \rangle$ crystal directions, although for some materials, the growth is along different axes at higher supersaturation.[18] These branches are approximately stationary in the laboratory frame of reference, and have a mean initial wavelength that is a few times the tip radius. Further behind the tip,

the side branches compete in a complex coarsening process that is not well understood.

In the standard continuum model of dendritic crystal growth from solution, the growth of the crystal is assumed to be limited by the diffusion of the depositing substance towards the interface.[2] Since thermal diffusion is much faster than chemical diffusion, the latent heat of crystallization may be neglected. The solid-liquid interface is assumed to be microscopically rough, macroscopically curved, and approximately at thermodynamic equilibrium. Furthermore, the solid is assumed to expel all of the water. This leads to the "one-sided" model of solidification. (The "symmetric" model applies to the growth of a pure substance from the melt, where the growth is limited by the diffusion of the latent heat of solidification, and where the solid and liquid thermal conductivities are taken to be equal. The symmetric model is approximately valid for succinonitrile.)

The concentration of the depositing substance in the solution $C(\mathbf{r})$ is expressed in terms of a dimensionless concentration field $u(\mathbf{r})$ given by

$$u(\mathbf{r})=\frac{C(\mathbf{r})-C_{\mathrm{eq}}}{\Delta C} ,$$

where C_{eq} is the equilibrium saturation concentration (mass per unit volume) at the operating temperature and $\Delta C=\rho_s-C_{\mathrm{eq}}$, where ρ_s is the density of the solid. In the solution, $u(\mathbf{r})$ satisfies the diffusion equation

$$D\nabla^2 u=\partial u/\partial t ,$$

where D is the diffusion constant for the depositing substance in solution.

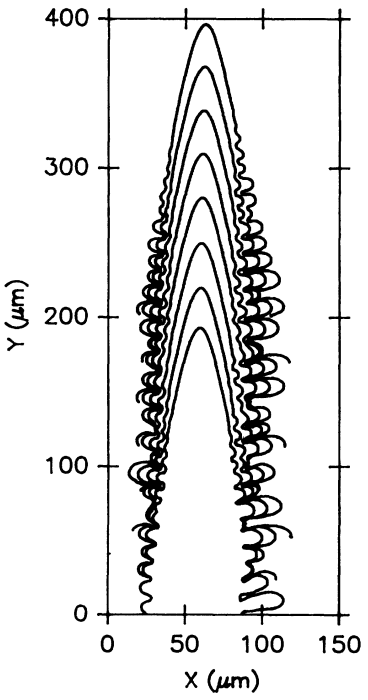

FIG. 1. Contours of a growing dendrite taken at 10-s intervals.

If the surface tension is isotropic, the concentration at the interface is given by the Gibbs-Thompson relation[2]

$$u_i=d_0\kappa ,$$

where κ is the curvature and d_0 is the capillary length. If the surface tension is anisotropic, however, the Gibbs-Thompson relation must be modified, and the concentration at the interface is then[10]

$$u_i=d_0(\theta_1,\theta_2)(\kappa_1+\kappa_2)+\frac{\partial^2 d_0(\theta_1,\theta_2)}{\partial^2\theta_1}\kappa_1 + \frac{\partial^2 d_0(\theta_1,\theta_2)}{\partial^2\theta_2}\kappa_2 , \quad (1)$$

where θ_1 and θ_2 are angular displacements along the principal axes of the surface and κ_1 and κ_2 are the corresponding principal curvatures. The capillary length $d_0(\theta_1,\theta_2)$ is given in terms of the surface tension $\gamma(\theta_1,\theta_2)$ and the chemical potential μ of the depositing substance by[2]

$$d_0(\theta_1,\theta_2)=\frac{\gamma(\theta_1,\theta_2)}{(\Delta C)^2(\partial\mu/\partial C)} .$$

For a crystal with cubic symmetry, the surface tension in the (100) plane is assumed to be of the form[1]

$$\gamma(\theta)=\gamma_0[1+\varepsilon_4\cos(4\theta)+\cdots] , \quad (2)$$

where θ is the angle from the [100] direction, and the dots indicate higher harmonics. In the same plane, the angular dependence of the capillary length is then

$$d_0(\theta)=\bar{d}_0[1+\varepsilon_4\cos(4\theta)+\cdots] ,$$

where $\bar{d}_0$ is the average of $d_0(\theta)$ over all angles.

Far from the interface, the concentration tends to the asymptotic value $u_\infty=\Delta$, where Δ is the supersaturation. Finally, from conservation of mass, the normal velocity of the interface is

$$v_n=D\nabla u\cdot\mathbf{n} , \quad (3)$$

where $\mathbf{n}$ is a unit vector normal to the interface.

B. Dendritic growth

In the limit of vanishing surface tension, the steady-state shape of the growing crystal is given by the Ivantsov solution, a paraboloid of revolution propagating at constant speed,[19] or by a needle crystal of elliptical cross section.[20] The dendrite tip speed and radius of curvature are given in terms of the supersaturation by

$$\Delta=pe^p E_1(p) ,$$

where $p=\rho v/2D$ is the Péclet number and $E_1(p)$ is the exponential integral. A continuous family of solutions exists, so that for a given Δ, no unique prediction can be made for the tip radius and speed.

Experimentally, however, a unique tip radius and speed are found[3–7] at a given supersaturation. The experiments of Huang and Glicksman[5] on succinonitrile further established that the combination $v\rho^2$ is approxi-

mately constant. This fact may be expressed by introducing a dimensionless stability constant

$$\sigma^* = \frac{2\bar{d}_0 D}{v\rho^2} . \tag{4}$$

For succinonitrile, σ^* was found[5] to be 0.0195. This value is roughly consistent with the hypothesis that the dendrite tip is marginally stable (perturbations that deform the tip have precisely zero growth rate).[2,21] The quantity $v\rho^2$ was also found to be approximately constant for the growth of NH_4Br dendrites from aqueous solution in a capillary tube,[7] but lack of knowledge of the materials parameters prevented a quantitative determination of σ^*. Similar results were also found[22] for the dendritic growth of ^4He. However, this quantity was not found to be a constant in the dendritic growth of krypton.[23] This was attributed to the importance of attachment kinetics in that system.

Recent theoretical work has shown that if isotropic surface tension is included, there are no steady-state solutions. However, when a finite anisotropy is included in $\gamma(\theta)$, a discrete set of solutions is found.[1,8] Of this set, only the one with the highest speed is linearly stable.[9] This solution is a needle crystal that is approximately parabolic close to the tip, and corresponds to a particular value of σ^* that depends only on the crystalline anisotropy. In the region of experimental interest, where $\varepsilon_4 \approx 0.01$, the value for σ^* obtained from numerical calculations is found to vary approximately linearly with ε_4.

It may also be possible to explain side branching within this theoretical framework by considering the effect of finite amplitude perturbations on the tip.[10–16] In a frame of reference moving with the tip, a perturbation appears as a wave that propagates along the dendrite away from the tip. Periodic perturbations are strongly amplified for a broad range of wavelengths.[13,14] If λ is estimated to be the wavelength of the fastest growing perturbation, then the ratio λ/ρ depends only on the crystalline anisotropy.[13,14] However, this wavelength increases slowly as the perturbation moves away from the tip, so there is no completely unambiguous way to identify the side-branch wavelength from this calculation.[14] Furthermore, for any given initial wavelength, there is a distance behind the tip at which the perturbation will stop growing,[14] while in experiments, side branches continue to grow at all distances behind the tip. Calculations on the evolution of a perturbation containing a range of wavelengths,[14] on the other hand, show that if the initial perturbation contains arbitrarily long wavelengths, then it will continue to grow at arbitrary distances behind the tip. In this model, the estimated side-branch wavelength is still weakly dependent on the distance behind the tip, but the ratio λ/ρ is found to be approximately proportional to $(\sigma^*)^{1/2}$. A similar result for λ/ρ has also been obtained by considering the evolution of a disturbance that is initially localized near the tip.[16]

C. Growth of a small, nearly spherical crystal

The key difficulty in making a quantitative comparison with theory is the need for accurate measurements of the capillary length $\bar{d}_0$ and the surface tension anisotropy ε_4. Both of these quantities can be determined by considering the properties of a small, nearly spherical crystal that is approximately in equilibrium with the solution.

In the quasi static approximation,[2] the concentration outside an isolated sphere of radius R held at constant temperature is assumed to satisfy $\nabla^2 u(\mathbf{r})=0$. For the determination of $\bar{d}_0$, we ignore the small anisotropy, so that at the interface $u(R)=2\bar{d}_0/R$. The concentration field is then

$$u(\mathbf{r}) = \Delta - \frac{R}{r}\left[\Delta - \frac{2\bar{d}_0}{R}\right] ,$$

and the radial velocity is

$$v_R = \frac{D}{R}\left[\Delta - \frac{2\bar{d}_0}{R}\right] . \tag{5}$$

The capillary length can be determined by fitting Eq. (5) to the measured rate at which a crystal shrinks when it is close to equilibrium, with the right-hand side of Eq. (5) slightly negative. (A growing crystal cannot be used for this measurement because it would eventually become morphologically unstable.[2]) This method for determining $\bar{d}_0$ assumes that kinetic effects do not create an asymmetry between the processes of growth and dissolution of a rough interface, an assumption that is discussed in Sec. II D and is consistent with the anisotropy results reported in Sec. IV.

The anisotropy in $\gamma(\theta)$ can be determined from measurements of the shape of a single crystal in equilibrium with the solution. If the surface tension $\gamma(\theta)$ is given by Eq. (2), then the radius of the crystal measured in the (100) plane will be[10]

$$R(\theta) \approx R_0[1+\varepsilon_4\cos(4\theta)+\cdots] . \tag{6}$$

Since the second derivative of $d_0(\theta)$ enters the expression for u_i in Eq. (1), it is important to place limits on any higher harmonics in $R(\theta)$. Because the equilibrium state of Eq. (5), $v_R=0$, is unstable, it is in practice necessary to measure the anisotropy of a slowly shrinking crystal (or possibly a very slowly growing one).

D. Assumptions

In all of the theoretical work we have summarized, it is assumed that the interface of the growing dendrite is rough on a microscopic scale. Furthermore, in order to determine the anisotropy in the surface tension, it is assumed that the equilibrium shape of the crystal is not faceted.[24] This will be true for some materials if the temperature is sufficiently high.[25] However, under certain conditions, the assumption is violated by other materials that grow dendritically, including NH_4Br in solution. Crystals of these materials held in equilibrium will eventually become at least partially faceted. However, when driven slightly away from equilibrium (by growth), the facets disappear,[26] and the interface becomes macroscopically curved. We refer to this phenomenon as kinetic roughening. Although not much is known about kinetic

roughening, we propose as a working hypothesis that the properties of a kinetically roughened interface are indistinguishable from those of a thermally roughened interface. If so, the standard continuum model of dendritic growth described above should apply to the kinetically roughened interface as well.

The method we have adopted to measure the capillary length requires symmetry between the growth and dissolution kinetics. For a faceted interface, this is generally not the case. Instead, growth takes place primarily at steps at the edges of screw dislocations or at nuclei on the surface, while dissolution is dominated by the removal of molecules from corner sites.[27] This asymmetry is clearly evident in the crystal shape, since growing crystals often have sharp corners, while dissolving ones have rounded corners. Thus the anisotropy in the crystal shape will in general depend on the growth velocity of the crystal. For a rough interface, however, there is no nucleation barrier, and growth and dissolution take place at similar sites.[27] Thus for a rough interface, it is reasonable to assume that both the growth and the dissolution rates of an approximately spherical crystal are given by Eq. (5), and that the shape anisotropy will not depend on the velocity (provided it is sufficiently slow that the quasistatic approximation still applies). Furthermore, we propose that this symmetry between growing and shrinking is applicable to kinetically roughened crystals such as NH_4Br. The anisotropy measurements described in Sec. IV support these hypotheses.

Finally, the continuum growth model requires that the tip radius be sufficiently large compared to the atomic scale that microscopic irregularities and thermal fluctuations are insignificant. (Although fluctuations are sometimes introduced to explain side branching, their effects on the size and stability of the tip are usually assumed negligible.) This assumption may not be completely adequate when the tip radius is at the micron level or smaller, as occurs for growth from solution at sufficiently large supersaturation.

III. EXPERIMENTAL METHODS

A. Crystal growth

The crystal growth cell is a rectangular glass cylinder $60\times10\times1$ mm^3 that is initially open at both ends. Thin cells are used to accommodate the 7.5-mm working distance of the microscope objective and to suppress convective flow in the fluid. One end of the cell is filled with a tapered wedge of glass and sealed with a gap-filling, water-resistant epoxy. Analytical reagent grade NH_4Br (99.7% pure) is combined with distilled, deionized water that has been filtered through a 0.22-μm membrane filter. (The main impurity in the NH_4Br is 0.2% chloride, which is difficult to remove.) The NH_4Br is dissolved in the water in a beaker held well above the saturation temperature. The cell is then immersed in the solution and filled. An air bubble is left in the cell to be used as a stirrer, and the remaining open end of the cell is sealed in the same manner as the first. In most of the experiments reported here, the saturation temperature was 56 °C, and the solution consisted approximately of 51% NH_4Br by weight. Under these conditions, the diffusion constant for NH_4Br in solution is $D=2600\pm200$ μm^2/s.

To obtain steady-state growth, the solution must be held at constant temperature. The growth cell is placed in a groove $\frac{1}{8}$-in. deep inside a copper block whose temperature is electronically controlled to about 2 mK. This corresponds to fluctuations of approximately 3×10^{-6} in Δ. A vertical hole in the block, covered with glass windows, is used for optical access on an Olympus inverted microscope. For additional thermal stability, the bottom of the block is insulated from the microscope stage, and the top is covered with a temperature-regulated aluminum heat shield.

To initiate growth, the solution is heated above the saturation temperature T_{sat} and stirred thoroughly. A crystal is then nucleated by cooling one end of the cell. Once growth begins, the temperature is set approximately to T_{sat}, and the cell is allowed to equilibrate. The crystal may be placed in a favorable orientation by momentarily tilting the cell. Dendritic growth is initiated by gradually cooling the cell to a few degrees below T_{sat}, so that Δ is on the order of 0.01. Only experiments in which a single dendrite grows far from any other crystals are used for analysis.

Small crystals for the capillary-length and surface-tension measurements can be obtained by slowly raising the temperature of a growing dendrite to slightly below the saturation temperature. This results in a large dendrite tip. As the temperature rises, the sharply curved parts of the dendrite begin to dissolve, leaving only the tip and the largest side branches. These crystals eventually become approximately spherical. The temperature is then held constant. If there are several crystals in the cell, only isolated ones are considered. The growth or shrinking of the crystal is recorded on videotape at regular intervals under computer control.

B. Image analysis

The growth cell is observed using a 10 or 20 power objective. The microscope also has an optional 1.5-power stage multiplier lens. The image is sent through a 6.7-power photo eyepiece to a videocamera, where it is recorded on standard VHS videotape for subsequent analysis. The videotape is played back under computer control, and images are digitized at a resolution of 512 by 480 picture elements (pixels) using digitizing boards from Imaging Technology, Inc. Real-time image averaging is performed to reduce noise. The overall magnifications range from approximately 1 to 0.32 μm/pixel, and the distortion in linear measurements is less than 1%.

The location of the solid-liquid interface can be measured to a precision considerably better than the pixel size in the following manner.[17] The light intensity in the digitized image drops sharply from I_{out} to I_{in} over a distance of about 5 pixels (Fig. 2) as the interface is crossed from the exterior to the interior of the dendrite. The intensity function is approximated by a straight line in the interfacial region. The location of the interface is taken to be the intersection of that straight line with an intensi-

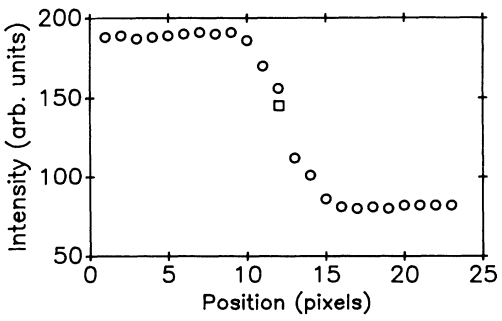

FIG. 2. Intensity in the digitized image across the dendrite interface. The square shows the interpolated interface position (see text). The digitization unit, 1 picture element (pixel), corresponds to 0.32 μm.

ty threshold $I_{in}+f(I_{out}-I_{in})$, where f is a fractional threshold, typically taken to be 0.6. This interpolation procedure yields an uncertainty in measurements of the dendrite tip radius of about 0.1 pixel. For the highest magnifications, this corresponds to about 0.03 μm, considerably less than optical wavelengths. For consistency, the image is always scanned in a direction approximately perpendicular to the interface, and a threshold of $f=0.6$ is always used, although the results are generally not sensitive to these factors.

IV. EXPERIMENTAL RESULTS

The crystal morphology is strongly dependent on both the saturation temperature T_{sat} and the supersaturation Δ. In the temperature range used in this experiment, the equilibrium shape of a small NH_4Br crystal is partially faceted. However, microscopically rough (and macroscopically curved) interfaces can be obtained by raising Δ such that the interface grows and kinetic roughening occurs. The growth speed required to produce kinetic roughening decreases with increasing T_{sat}. If T_{sat} is approximately 55 °C, then kinetic roughening is observed for interfacial speeds on the order of 10^{-3} μm/s, while if T_{sat} is approximately 90 °C, then kinetic roughening is observed for speeds of 10^{-4} μm/s. At the higher temperatures especially, the transition to a faceted structure as the growth speed is lowered takes place very slowly, such that even with an average interfacial velocity on the order of 10^{-5} μm/s, a 20-μm crystal is only partially faceted after several hours. It is difficult to maintain such small growth rates over sufficiently long times to completely characterize the transition. A similar "dynamic broadening" of the roughening transition has been observed in other systems,[28] such as solid ^{3}He. All the measurements reported here were made on macroscopically curved interfaces that are assumed to be microscopically rough.

A. Capillary length $\bar{d}_0$

The capillary length may be determined by measuring the rate at which a small, nearly spherical crystal shrinks when the difference $\Delta-2d_0/R$ is very small, about 10^{-5} in the present experiment. If the temperature is raised slightly while a faceted crystal is present in the cell, the corners of the crystal are the first parts to dissolve. The crystal soon becomes approximately spherical, and begins to shrink. If the radial velocity is large enough that kinetic roughening occurs, but small enough that the quasistatic approximation is still valid, then Eq. (5) will apply.

The contours of a slowly shrinking crystal with $T_{sat}\approx 46$ °C are shown in Fig. 3 at 10-min intervals. The crystal is viewed from below, so the contours represent projections of the crystal on the horizontal plane. The crystal appears to remain roughly spherical throughout the entire process, although it may still be slightly elongated along the original dendrite growth direction, and some evidence of faceting remains at early times. The mean radius $R(t)$ of the projection of the crystal is obtained by averaging the radius over all angles. The time dependence of $R(t)$ is then measured (Fig. 4) in order to determine the capillary length $\bar{d}_0$.

For a free sphere in an infinite solution, $R(t)$ is given by integrating Eq. (5) above. In the actual experiment, however, the shrinking crystal rests on the bottom of the growth cell. This imposes the additional constraint that the gradient of the concentration perpendicular to the wall must be zero. As a result, the growth rate is reduced. Although the crystal shape is not known, we have treated the process in the following approximate manner. The concentration field outside a sphere tangent to a wall is calculated numerically in the quasistatic approximation by solving Laplace's equation on a large (75 000 point) grid using an over-relaxation algorithm. The result is shown in Fig. 5, where contours of constant concentration in a vertical plane are shown for a sphere of unit radius resting on the cell bottom. The mass flux dm/dt away from the sphere is determined by integrating the concentration gradient over a hemisphere that encloses the crystal. If we assume that the crystal remains spherical, then the radial velocity $v_R=dR/dt$ is related to the mass flux by $dm/dt=(4\pi R^2)dR/dt$. The overall result is that v_R is reduced by a factor of 0.71 from Eq. (5).

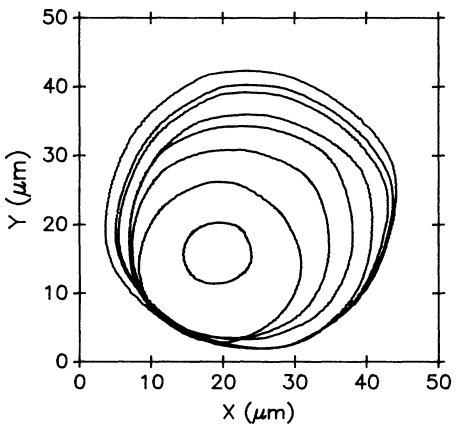

FIG. 3. Contours of a shrinking crystal at 10-min intervals. The crystal appears to move somewhat, as discussed in the text.

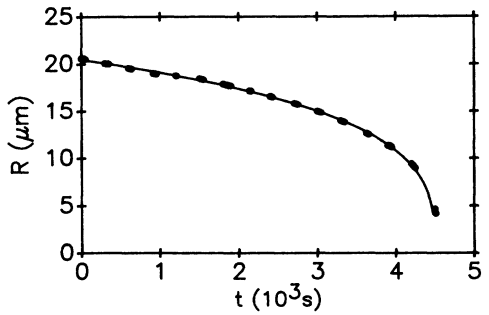

FIG. 4. Time dependence of the average radius of the crystal in Fig. 3. The solid line is a fit to Eq. (5), corrected for the presence of the cell wall (see text), with capillary length $\bar{d}_0 = 2.8 \times 10^{-4}$ μm, and $\Delta = 1.4 \times 10^{-5}$.

The actual crystal may not stay spherical, however. If we start with a sphere in the numerical calculation, we find that it shrinks most rapidly on the top and flattens slightly, at least initially. We have not followed the evolution of the shape numerically beyond this initial state. In the experiment, the crystal tends to move somewhat, as is evident in Fig. 3. This motion may contribute to keeping the crystal approximately spherical. The crystal could roll if the cell is not perfectly level, or if the subsequent evolution of the crystal leads to an unstable shape. We expect, however, that any additional corrections to the radial speed due to shape changes would not significantly change the results for $\bar{d}_0$, within the experimental precision.

The best fit to the data in Fig. 4 gives $\bar{d}_0 = 2.8 \pm 0.4 \times 10^{-4}$ μm, where the uncertainty represents a 90% confidence level due to statistical errors. The quality of the fit also confirms that the shrinking of the crystal is well described by the quasistatic approximation for the diffusion-limited growth of a rough interface.

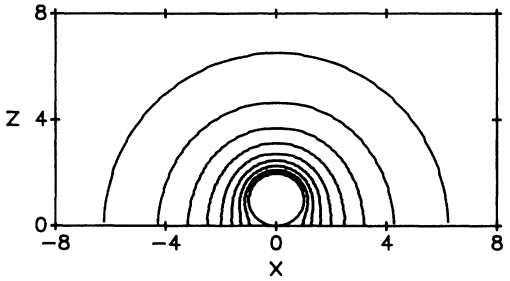

FIG. 5. Computed contours of constant concentration for a sphere on the bottom of the cell in the quasistatic approximation. The dimensionless concentration at the sphere is normalized to 1. Successive contours are at intervals of 0.1.

B. Crystalline anisotropy

To determine the anisotropy in the surface tension, the radius of a single crystal is measured as a function of angle. We observe a kinetically roughened crystal in order to determine the surface tension anisotropy appropriate to the growing dendrite, since that of the faceted equilibrium crystal would not apply. Comparison of the results for a slowly growing and a slowly shrinking crystal also allows a test of the symmetry between these two cases. This symmetry is important for interpreting the results of the capillary-length measurement above.

The radius as a function of angle for a slowly shrinking crystal from Fig. 3 is shown in Fig. 6(a). The crystal is shrinking rapidly enough that kinetic roughening has occurred. The fourfold anisotropy coefficient in Eq. (6) may be determined from a Fourier series representation of $R(\theta)$, as shown in Fig. 6(b). Averaging the results from three different crystals, we find that $\varepsilon_4 = 0.016 \pm 0.004$. In addition, the ratio $\varepsilon_8/\varepsilon_4$ is estimated to be less than about 0.2.

To test whether the same anisotropy is obtained for growing and shrinking crystals, we have measured the shape anisotropy of a crystal near $T_{sat} \approx 90$ °C. At the higher temperature, kinetic roughening occurs at a much lower interfacial speed, so a kinetically roughened growing crystal can be studied before it becomes morphologically unstable. A crystal of radius $R \approx 26$ μm was held approximately in equilibrium in solution. Over the course of about an hour, the radial velocity v_R ranged between roughly -5×10^{-4} and 5×10^{-4} μm/s. Over this

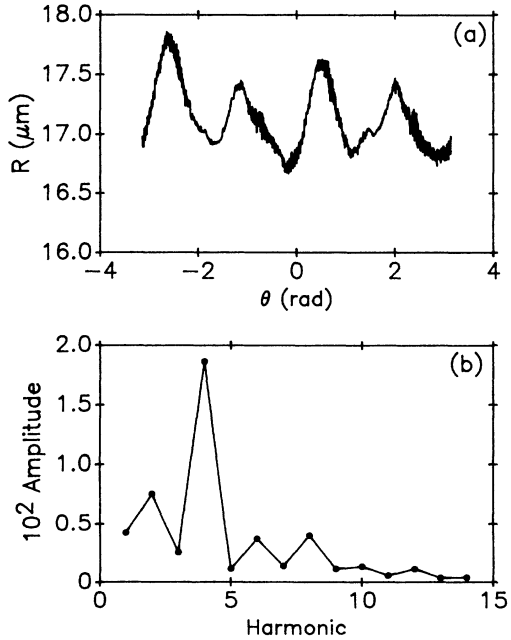

FIG. 6. (a) Radius vs angle for a single crystal approximately in equilibrium with the solution. (b) Amplitudes of the first few coefficients in a Fourier series representation of $R(\theta)$.

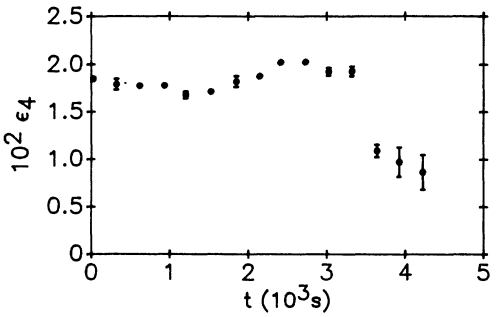

FIG. 7. Time dependence of the apparent anisotropy ε_4 for the crystal in Figs. 3 and 4. The measurement is valid for $t \lesssim 3000$ s, when the crystal begins to move.

time interval, the shape anisotropy was $\varepsilon_4 = 0.016 \pm 0.002$. Similar measurements were made for another crystal with v_R between -0.007 and 0.007 μm/s over an interval of about 1.5 h, and the shape anisotropy was found to be $\varepsilon_4 = 0.016 \pm 0.003$. These results are consistent with the hypothesis of symmetry for the growing and shrinking of kinetically roughened crystals, and they support the use of the capillary length determined from a shrinking crystal to characterize the growing dendrite.

It is important to know the orientation of the crystal axes in order to measure the anisotropy. Since the crystal was originally part of a dendrite growing in the horizontal plane, the [100] direction corresponding to the main dendrite stem is also in the horizontal plane. The [010] direction corresponding to one set of side branches is also approximately in the horizontal plane, so that the normal to the image must be nearly along the [001] direction, although the orientation is not precisely known. The differences in height of the four peaks in Fig. 6(a) may be due, in part, to an error in alignment of the crystal.

The time dependence of ε_4 for the crystal in Fig. 3 is shown in Fig. 7. Although the shrinking crystal is not in equilibrium, we find that as long as the radial speed is fairly small and the crystal has not rolled significantly, the measured ε_4 is approximately constant. This indicates that ε_4 does not depend on interfacial velocity. The apparent ε_4 begins to decrease after about $t = 300$ s, due to the motion visible in Fig. 3, so that the crystal is no longer being viewed along the [001] direction. Prior to that time, the alignment is estimated to be correct to within about 20°, so that orientational error should reduce the apparent anisotropy at worst by a factor of 0.94.

C. Steady-state dendritic tips

Given the measured value of $\bar{d}_0$ obtained above, the stability constant σ^* can be computed from measurements of the steady-state tip radius and speed over a range of supersaturations. For each supersaturation, a series of images of the growing dendrite tip is digitized at regular intervals. For each image, a parabola is fitted to the tip to determine the tip radius and position. The speed is measured by dividing the tip displacement between two images by the time interval. This analysis is then repeated on a number of images to determine the steady-state values of ρ, v, and σ^*.

The contour of a dendrite growing at $v = 3.1$ μm/s is shown in Fig. 8, along with a parabola of radius $\rho = 2.1$ μm fitted to the tip. The parabola is fitted in the following manner. Approximately 50 to 80 points along the interface, from the tip to a distance of about 3ρ behind the tip, are found by scanning along horizontal and vertical lines in the digitized image and using the interface-finding algorithm described above. A parabola is then fitted to these points to estimate the tip location and radius, and the orientation angle of the dendrite. Since the interface is sharply curved near the tip, the horizontal and vertical scans do not generally give a highly accurate measurement of the tip location and radius. However, using this as a first approximation, a new set of points is found, this time always reading the image intensity on a line approximately perpendicular to the interface. The result is a substantially improved measurement of the interface. This process is repeated several times until subsequent iterations do not decrease the uncertainty in ρ. For the dendrites measured in this experiment, the typical tip radius is about 10 pixels, with an uncertainty of about 0.1 pixel.

The accuracy of the fit may be assessed in several ways. First, the measured tip radius may be determined as a function of the maximum distance z_{max} behind the tip used in the fitting process. The measured radius is found to be a slowly increasing function of z_{max} [Fig. 9(a)], due to the fact that the dendrite is only approximately parabolic. For $z_{max} \gtrsim 4\rho$, the tip of the best fitting parabola begins to deviate noticeably from the actual tip of the dendrite, even though no side branches can be detected at that distance. A second approach to assessing the quality of the fits is to determine the reduced χ^2, as shown in Fig. 9(b). This quantity gradually increases with z_{max} but does not give a sharp criterion for the optimal z_{max}. One cannot choose z_{max} to be less than about 2ρ because the number of data points becomes small, causing the uncertainty to increase, as indicated by the bars in Fig. 9(a). Also, the sharply curved tip region is the most difficult part of

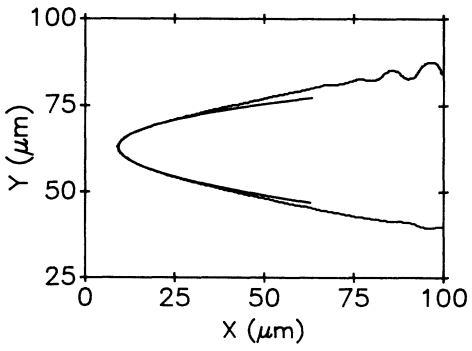

FIG. 8. Tip of a dendrite with a parabola of radius $\rho = 2.1$ μm fitted to the tip.

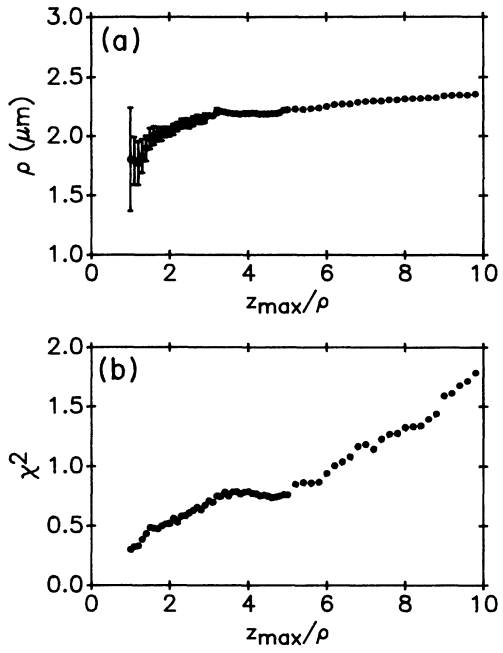

FIG. 9. (a) Measured tip radius as a function of the maximum distance z_{max} used in the fit. The apparent radius increases steadily as points further back along the dendrite are included. (b) Reduced χ^2 for the parabolic fit. Based on these results, we chose $z_{max}=3\rho$ for all tip-radius measurements.

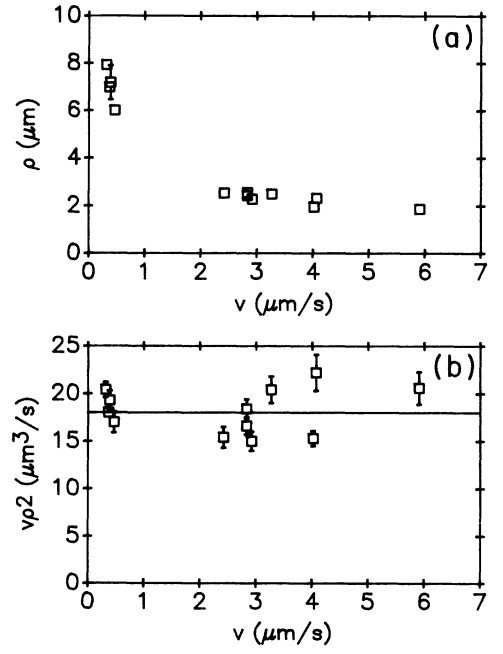

FIG. 10. (a) Steady-state values of ρ as a function of tip speed v, for a number of dendrites. (b) Steady-state value of $v\rho^2$ for the same dendrites. The average value (solid line) is 18 ± 3 $\mu m^3/s$, whereas the theoretical prediction is 22 ± 7 $\mu m^3/s$.

the dendrite to image accurately. As a reasonable compromise, we have chosen $z_{max}=3\rho$.

The steady-state growth of several different dendrites is represented in Fig. 10(a), where we have plotted ρ versus v, and in Fig. 10(b), where we have plotted $v\rho^2$ versus v. Though there is significant scatter, $v\rho^2=18\pm3$ $\mu m^3/s$, and is approximately constant. Using the value for $\bar{d}_0$ obtained above, we find from Eq. (4) that $\sigma^*=0.081\pm0.02$.

D. Measurement limitations

We are able to perform accurate measurements only over a somewhat restricted range of velocities. At high velocities, the dendrite tips become too small to be accurately measured. Even at the highest available magnification, a tip radius of 2 μm corresponds to only 6.25 pixels. This may account for the somewhat larger scatter in the data at high speed.

At low velocities, two additional effects may become important. First, the characteristic length of the diffusion field $l=2D/v$ becomes larger than the cell thickness $d=1$ mm. However, as shown in Ref. 17, this does not seem to be an important effect. For the data in Fig. 10, the ratio l/d varies from 0.92 to 16, but there is no clear dependence of $v\rho^2$ on l/d. A second effect that must be considered is convection in the fluid due to horizontal density gradients near the interface. In the experiments on succinonitrile at very low supercoolings,[5] the growth speed depended strongly on the orientation of the dendrite with respect to gravity. This was attributed to convective flow in the fluid. In the present experiments, on the other hand, the thin horizontal cells should strongly suppress convective flow. We observed no evidence of buoyancy-induced convection.

Bulk fluid flow could also occur as a result of the density change upon crystallization. For the NH_4Br system, however, this effect is small. If the excess NH_4Br in a fixed quantity of supersaturated solution at $\Delta=0.01$ is crystallized, the relative density change is $\delta=(\rho_f-\rho_i)/\rho_i\approx0.006$, where ρ_i is the density of the initial solution and ρ_f is the average density of the final solid-liquid mixture. In the symmetric model for solidification from the melt, neglecting surface tension, McFadden and Coriell[29] have shown that a small density change upon crystallization only acts as a small perturbation of order δ to the Ivantsov solution, and is negligible for many materials of interest. For succinonitrile, in comparison, δ is 0.028.

Finally, because small changes in impurity concentration might have a significant effect on the material properties, all the dendrite measurements reported here were performed on the solution in a single sealed cell, although measurements in other cells gave similar results. The anisotropy measurements in several different cells all gave comparable results.

E. Time evolution of $v\rho^2$

As an additional check on the combination $v\rho^2$, we monitor the growth of a single dendrite as a function of

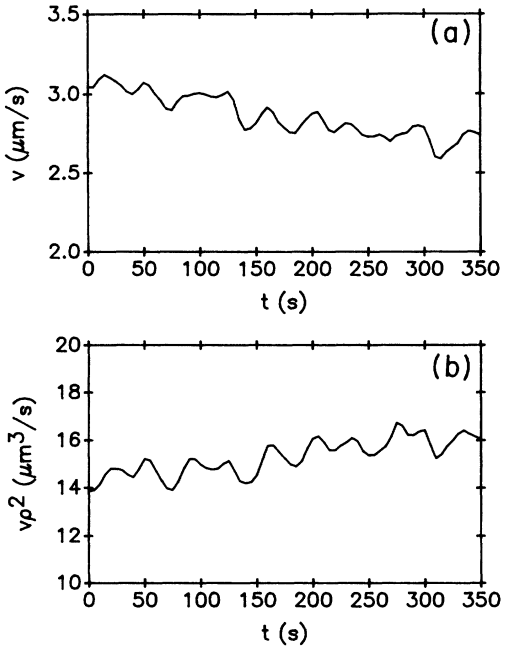

FIG. 11. (a) Time dependence of tip speed for a single dendrite. The dendrite gradually slows down due to finite size effects. (b) Time dependence of $v\rho^2$ for the same dendrite. The small drift due to finite size effects is not a dominant source of error.

time. In a finite cell, the dendrite need not reach a strictly steady state, since the cell gradually becomes depleted, and the cell walls can also affect the diffusion field. Such finite size effects have been studied theoretically[30] to a limited extent, but are not well understood. We observe that over long times the dendrite speed tends to decrease, as shown in Fig. 11(a). (The fluctuations in the graph reflect the measurement uncertainties in both v and ρ.) The combination $v\rho^2$ increases slowly with time [Fig. 11(b)], but the total drift is no larger than the variation from one run to another. This suggests that the quantity $v\rho^2$ is a fairly robust measure of the dendrite-tip properties even if the growth conditions are not strictly steady.

F. Side-branch spacing

We have also tested the hypothesis that λ varies linearly with ρ. In previous work,[17] we showed that the side branching is only roughly periodic, even quite close to the tip. For this reason, the mean wavelength must be determined from measurements of a large number of side branches. It is convenient to determine λ in the same manner as in Ref. 17. In a frame of reference moving with the tip, the side branches appear as propagating waves. The half-width of the dendrite $w_z(t)$, measured from the center to one side at a fixed distance z behind the tip, is an oscillating function of time. The side-branch wavelength is determined by dividing the tip speed by the mean frequency of the peak in the power spectrum of $w_z(t)$. This gives a statistically stationary measure of λ.

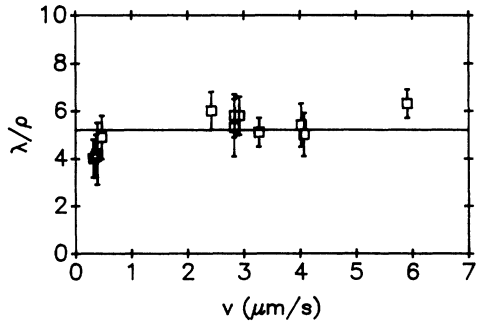

FIG. 12. Ratio of the mean initial side-branch wavelength to the tip radius for the dendrites in Fig. 10. The average value (solid line) is 5.2, whereas the theoretical prediction is 3.7.

The ratio λ/ρ is shown in Fig. 12 for the dendrites whose steady-state tip properties are given in Fig. 10. We find that $\lambda/\rho \approx 5.2 \pm 0.8$, and is approximately constant. However, as in Ref. 17, we also find that the side-branch spacing is irregular, and the power spectrum of $w_z(t)$ has a broad peak at the mean side-branching frequency.

V. COMPARISON WITH THEORY

The theoretical model predicts that σ^* is a strong function of the surface tension anisotropy. Using the experimentally measured value of $\varepsilon_4 = 0.016 \pm 0.004$ in the one-sided model of solidification, Kessler and Levine[31] predict that $\sigma^* \approx 0.065 \pm 0.02$, where the uncertainty is primarily due to that in ε_4. This prediction compares favorably with the experimental value of $\sigma^* = 0.081 \pm 0.02$. For the same anisotropy, the theoretically estimated value for the mean initial side-branch spacing is $\lambda/\rho \approx 3.7$. As noted above, the estimate is somewhat dependent upon the particular details of the model, but is smaller than the experimental value of $\lambda/\rho \approx 5.2 \pm 0.8$.

In order to make a quantitative comparison of these results with the experiments on succinonitrile, the differences between the one-sided and symmetric models, and the scaling of the dendrite properties with anisotropy, must be considered. For the one-sided model in two dimensions, the predicted value of σ^* is twice that for the symmetric model with the same anisotropy.[32] Similar results are expected to hold in three dimensions.[31] In addition, σ^* is predicted to scale roughly linearly with ε_4, for $\varepsilon_4 \approx 0.01$.

The anisotropy for succinonitrile[6] is approximately $\varepsilon_4 \approx 0.005$, but no uncertainty is quoted in Ref. 6. The ratio of the stability constant for ammonium bromide to that of succinonitrile is then predicted to be

$$\frac{\sigma_a^*}{\sigma_s^*} \approx (2)\frac{\varepsilon_a}{\varepsilon_s} = 6.4 \pm 1.6 ,$$

where the uncertainty is that in ε_4 for NH_4Br. The stability constant for succinonitrile is found[5] to be $\sigma_s^* = 0.0195$. The ratio of the experimentally determined

stability constants is thus 4.1 ± 1, somewhat smaller than the expected value. This reflects the fact that the experimental value of σ_s^* is larger than that predicted by the theory.

The estimates of the side-branch wavelength are the same for both the one-sided and symmetric models.[31] For $\varepsilon_4 \approx 0.01$, λ/ρ is expected to scale roughly with $(\varepsilon_4)^{1/2}$. For the two materials, the expected ratio of side-branch spacings is then

$$\frac{(\lambda/\rho)_a}{(\lambda/\rho)_s} \approx \left[\frac{\varepsilon_a}{\varepsilon_s}\right]^{1/2} = 1.8\pm0.2 \ .$$

The ratio of the side-branch wavelength to tip radius for succinonitrile is measured[6] to be $(\lambda/\rho)_s \approx 3$. The experimental ratio of side-branch spacings is thus 1.7 ± 0.3, in good agreement with the expected value.

We conclude that the experiments on NH_4Br are in approximate agreement with the predictions of the continuum model based on microscopic solvability for the dendrite tip radius and speed. The experimental mean initial side-branch spacing is somewhat greater than predicted, however. Furthermore, the values of σ^* and λ/ρ are larger for NH_4Br than for succinonitrile, in accord with the predicted trend with anisotropy, although the experimental value for the ratio of the two stability constants is smaller than expected. A more careful analysis of the differences between the one-sided and the symmetric models, and possibly a more precise determination of ε_4 for succinonitrile, are needed before a more quantitative comparison can be made.

The present theoretical models do not, however, address the complex time dependence of the side branching or the coarsening that occurs in the later stages of dendritic growth. If the side branching is noise driven, what is the origin of the noise? We find that the branching is an irregular process, even quite close to the tip where the side branches are only a few hundred angstroms long. At that length scale, the continuum model may no longer be accurate, and it may be necessary to consider number fluctuations of the NH_4Br molecules in solution. Indeed, the concentration fluctuations in a 1-μm^3 volume at $\Delta = 0.01$ give rise to fluctuations in Δ on the order of $(\delta\Delta/\Delta) \approx 10^{-3}$. The significance of these fluctuations, and their inclusion in the theory, are important areas for future study.[15,33]

ACKNOWLEDGMENTS

This research was supported by National Science Foundation (Low Temperature Physics Program) Grant No. DMR-85-03543. We thank H. Levine for providing predictions for the particular material used in these experiments and for helpful discussions. We also appreciate computing equipment provided by the U.S. Department of Defense University Research Initiative Program under Contract No. DARPA/ONR-N00014-85-K-0759 to Princeton University, and by the W. M. Keck Foundation.

[1]For recent reviews, see J. S. Langer, in *Chance and Matter,* Proceedings of the XLVI Les Houches Summer School of Theoretical Physics, 1986, edited by J. Souleti, J. Anninemus, and R. Stora (Elsevier, New York, 1987); D. A. Kessler, J. Koplik, and H. Levine, Adv. Phys. (to be published).

[2]J. S. Langer, Rev. Mod. Phys. **52**, 1 (1980).

[3]M. E. Glicksman, Mater. Sci. Eng. **65**, 45 (1984); M. E. Glicksman and N. B. Singh, in *Rapidly Solidified Powder Aluminum Alloys, ASTM SP 890,* edited by M. E. Fine and E. A. Starke, Jr. (American Society for Testing and Materials, Philadelphia, 1986), p. 44.

[4]M. E. Glicksman, R. J. Schaeffer, and J. D. Ayers, Metall. Trans. A **7A**, 1747 (1976).

[5]S.-C. Huang and M. E. Glicksman, Acta Metall. **29**, 701 (1981).

[6]S.-C. Huang and M. E. Glicksman, Acta Metall. **29**, 717 (1981). The anisotropy value of 0.01 quoted in this paper is $[R(0)-R(\pi/4)]/\langle R\rangle_{av}$, which is $2\varepsilon_4$.

[7]H. Honjo and Y. Sawada, J. Cryst. Growth **58**, 297 (1982).

[8]D. A. Kessler and H. Levine, Phys. Rev. A **36**, 4123 (1987); A. Barbieri, D. C. Hong, and J. S. Langer, Phys. Rev. A **35**, 1802 (1987); B. Caroli, C. Caroli, C. Misbah, and B. Roulet, J. Phys. **48**, 547 (1987); D. Meiron, Phys. Rev. A **33**, 2704 (1986); P. Pelcé and Y. Pomeau, Stud. Appl. Math. **74**, 245 (1986); M. Ben-Amar and Y. Pomeau, Europhys. Lett. **2**, 307 (1986).

[9]D. A. Kessler and H. Levine, Phys. Rev. Lett. **57**, 3069 (1986); P. Pelcé and P. Clavin, Europhys. Lett. **3**, 907 (1987); D. Bensimon, P. Pelcé, and B. I. Shraiman (private communication).

[10]D. A. Kessler and H. Levine (private communication).

[11]R. Pieters and J. S. Langer, Phys. Rev. Lett. **56**, 1948 (1986).

[12]Y. Saito, G. Goldbeck-Wood, and H. Muller-Krumbhaar, Phys. Rev. Lett. **58**, 1541 (1987).

[13]D. A. Kessler and H. Levine, Europhys. Lett. **4**, 215 (1987).

[14]M. Barber, A. Barbieri, and J. S. Langer, Phys. Rev. A **36**, 3340 (1987).

[15]J. S. Langer, Phys. Rev. A **36**, 3350 (1987).

[16]B. Caroli, C. Caroli, and B. Roulet, J. Phys. **48**, 1423 (1987).

[17]A. Dougherty, P. D. Kaplan, and J. P. Gollub, Phys. Rev. Lett. **58**, 1652 (1987).

[18]S.-K. Chan, H.-H. Reimer, and M. Kahlweit, J. Cryst. Growth **32**, 303 (1976).

[19]G. P. Ivantsov, Dokl. Akad. Nauk SSSR **58**, 567 (1947).

[20]G. Horvay and J. W. Cahn, Acta. Metall. **9**, 695 (1961).

[21]H. Muller-Krumbhaar and J. S. Langer, Acta. Metall. **29**, 145 (1981).

[22]J. P. Franck and J. Jung, J. Low Temp. Phys. **64**, 165 (1986).

[23]J. H. Bilgram, M. Firmann, and W. Kanzig, Phys. Rev. B **37**, 685 (1988).

[24]For a review of equilibrium crystal shapes, see M. Wortis, in *Chemistry and Physics of Solid Surfaces,* edited by R. Vanselow (Springer-Verlag, Berlin, in press), Vol VII.

[25]For a review of roughening, see J. D. Weeks, in *Ordering in Strongly Fluctuating Condensed Matter Systems,* edited by T.

Riste (Plenum, New York, 1980).
[26]P. Nozieres and F. Gallet, J. Phys. (Paris) **48**, 353 (1987); Y. Saito, in *Ordering in Strongly Fluctuating Condensed Matter Systems,* edited by T. Riste (Plenum, New York, 1980).
[27]G. S. Meiling and D. R. Uhlmann, Phys. Chem. Glasses **8**, 62 (1967).
[28]E. Rolley, S. Balibar, and F. Gallet, Europhys. Lett. **2**, 247 (1986).
[29]G. B. McFadden and S. R. Coriell, J. Cryst. Growth **7**, 507 (1986).
[30]D. A. Kessler and H. Levine, Phys. Rev. A **34**, 4980 (1986).
[31]H. Levine (private communication).
[32]C. Misbah, J. Phys. (Paris) **48**, 1265 (1987).
[33]J. Nittmann and H. Eugene Stanley, Nature **321**, 663 (1986); J. Nittmann and H. Eugene Stanley, J. Phys. (Paris) A **20**, L981 (1987).